A Letters Journal Exploring the Frontiers of Physics

October 2014

EPL, **108** (2014) 27007
doi: 10.1209/0295-5075/108/27007

www.epljournal.org

Spectroscopic signatures of the Mott transition on the anisotropic triangular lattice

Rajarshi Tiwari and Pinaki Majumdar

Harish-Chandra Research Institute - Chhatnag Road, Jhusi, Allahabad 211019, India

received 30 April 2014; accepted in final form 3 October 2014
published online 24 October 2014

PACS 71.30.+h – Metal-insulator transitions and other electronic transitions
PACS 71.27.+a – Strongly correlated electron systems; heavy fermions
PACS 74.25.Gz – Optical properties

Abstract – We use a new Monte Carlo method to study the Mott transition on the anisotropic-triangular-lattice Hubbard model. Our real space approach accurately treats the emergence of non-trivial magnetic correlation in this frustrated structure with reducing temperature. For hopping anisotropy typical of the two-dimensional organic salts, the coupling of electrons to self-generated magnetic moments leads to a pseudogap, huge d.c. resistivity, and non-Drude optical response over a wide temperature window. In addition to these generic signatures of a "bad metal", the spatial correlation among the magnetic moments leads to pronounced momentum dependence of quasiparticle extinction and pseudogap formation on the Fermi surface as the Mott transition is approached.

Introduction. – The Mott metal-insulator transition (MIT), and the proximity to a Mott insulator in doped systems, are crucial issues in correlated electron systems [1–4]. The Mott transition on a bipartite lattice is now well understood but the presence of triangular motifs in the structure brings in geometric frustration [5,6]. This promotes incommensurate magnetic fluctuations whose nature, and impact on the MIT, remain outstanding problems.

The organic salts provide a concrete realisation of this situation [7]. The active electronic sites in the quasi–two-dimensional material κ-(BEDT-TTF)$_2$Cu[N(CN)$_2$]-X live on a triangular lattice, with anisotropic hopping [8]. For X = $Cl_{1-x}Br_x$, varying x leads to a chemical-pressure–driven Mott transition [9]. Distinctive signatures near the Mott transition include a very incoherent [10] metal (with resistivity $\gtrsim 100\,\mathrm{m\Omega cm}$ above 50 K), non-Drude optical response [11,12], and the presence of a pseudogap in the density of states [13,14].

The dominant low-energy fluctuations near a Mott transition are magnetic and the features above would rise from electrons coupling to these modes. The nature of these modes remain a mystery. Variational Monte Carlo suggests that the magnetic correlations have a "spiral" character in the ground state [15] of the frustrated anisotropic lattice, but the fate of these correlations at finite temperature and their impact on electronic properties remain unresolved.

To address these issues we solve the Hubbard model on the anisotropic triangular lattice using an approach that retains extended spatial correlations, handles all thermal fluctuations, and allows access to spectral information across the MIT.

Choosing hopping anisotropy typical of the organics (see later), we discover the following. i) The magnetic fluctuations are peaked at a wave vector $\mathbf{Q} \sim (0.85\pi, 0.85\pi)$, away from the Néel state, and promote long wavelength spiral order in the Mott insulator at low temperature. ii) At intermediate temperature, the coupling of electrons to disordered local moments leads to strongly non-Drude optical response and a single-particle pseudogap —with both of these evolving into a gapped response deep in the Mott phase. iii) The electronic spectral function $A(\mathbf{k}, \omega)$ is *anisotropic* on the Fermi surface: a) the "hot" and "cold" spots are determined by the non-trivial magnetic wave vector $\mathbf{Q}$, b) there is a regime where the cold region shows a quasiparticle peak while the hot region already has a weak pseudogap, c) the anisotropy, indicative of a $\mathbf{k}$-dependent self-energy, is visible only at intermediate temperature —at high temperature the magnetic fluctuations are $\mathbf{q}$ independent, and at low temperature a gap opens all over the Fermi surface.

To set our results in context, there have been several studies of the single-band Hubbard model on a triangular lattice [16–28]. Dynamical mean-field theory (DMFT) has been the method of choice [20–22] for studying thermal properties, used sometimes in its cluster variant (C-DMFT) [23–26] to handle short-range spatial correlations. Other approaches focus on the ground state, using variational Monte Carlo (VMC) [15,17,19], variational cluster perturbation theory (VCPT) [27], or small-size exact diagonlisation (ED) [29].

These studies broadly suggest the following. i) The ground state is a paramagnetic metal (PM) at weak coupling, a "spin liquid" insulator at intermediate coupling, and an antiferromagnetic insulator (AFI) with Néel order ($\mathbf{Q} = (\pi, \pi)$) at large coupling U/t [16–19] up to large anisotropy t/t'. Some methods also predict [30–32] a low-temperature superconducting state near the Mott transition but this aspect is debated [29]. ii) There could be a re-entrant insulator-metal-insulator transition with increasing temperature for a certain window of frustration [24,25]. iii) The resistivity [20] and optical conductivity [11] have been obtained within DMFT, *i.e.*, without retaining any spatial correlations, and show features generic to any Mott transition.

There seems to be limited effort on clarifying the nature of *spatial fluctuations*, which could be significant in this low-dimensional frustrated system. At zero temperature, methods like ED [29], are severely size limited ($N \sim 4\times4$), and it is mostly from VMC [17,19] and path integral renormalization group (PIRG) [16,18] that some results are available. At large t'/t, these results indicate the transition from metal to non-magnetic insulator (PIRG), or to insulator with a spiral order (VMC), as opposed to Néel state, which survives up to $t'/t \sim 0.6$ in all results. These methods do not address transport and spectral features at finite temperature. C-DMFT [24–26] does access finite temperature and retains at least short-range spatial correlations but we are not aware of any transport results within this scheme.

Model and method. – Our real space framework aims to fill this gap: establishing the nature of magnetic correlations in this frustrated system, and their impact on the spectral properties. We study the following model:

$$H = \sum_{\langle ij\rangle\sigma} t_{ij} c^\dagger_{i\sigma} c_{j\sigma} - \mu \sum_i n_i + U \sum_i n_{i\uparrow} n_{i\downarrow}. \qquad (1)$$

We use a square lattice geometry but with the following anisotropic hopping: $t_{ij} = -t$ when $\mathbf{R}_i - \mathbf{R}_j = \pm\hat{x}a_0$ or $\pm\hat{y}a_0$, where a_0 is the lattice spacing, and $t_{ij} = -t'$ when $\mathbf{R}_i - \mathbf{R}_j = \pm(\hat{x}+\hat{y})a_0$. We will set $t = 1$ as the reference energy scale. $t' = 0$ corresponds to the square lattice, and $t' = t$ to the isotropic triangular lattice. We have studied the problem over the entire t'/t window $[0, 1]$, but focus on $t'/t = 0.8$ in this paper (results on the wider t'/t variation will be presented separately). μ controls the electron density, which we maintain at half-filling, $n = 1$. $U > 0$ is the Hubbard repulsion.

We use a Hubbard-Stratonovich (HS) transformation that introduces a vector field $\mathbf{m}_i(\tau)$ and a scalar field $\phi_i(\tau)$ at each site [33–36] to implement a rotation invariant decoupling of the Hubbard interaction. We can write $n_{i\uparrow}n_{i\downarrow} = \frac{n_i^2}{4} - (\vec{s}_i \cdot \hat{\mathbf{m}}_i)^2$ where $n_i = n_{i\uparrow} + n_{i\downarrow}$ is the charge density, $\vec{s}_i = 2\vec{\sigma}_i = \frac{1}{2}\sum_{\alpha,\beta} c^\dagger_{i\alpha}\vec{\sigma}_{\alpha\beta}c_{i\beta}$ is the local electron spin operator, and $\hat{\mathbf{m}}_i$ is an *arbitrary unit vector*. We introduce two space-time varying auxiliary fields i) $\phi_i(\tau)$ coupling to charge density, and ii) $\Delta_i(\tau)\hat{\mathbf{m}}_i(\tau) = \mathbf{m}_i(\tau)$ coupling to electron spin density (Δ_i is real positive). This allows the $SU(2)$ invariant HS transformation [33–36] (U being in units of t, is dimensionless)

$$e^{U n_{i\uparrow} n_{i\downarrow}} = \int \frac{\mathrm{d}\phi_i \mathrm{d}\mathbf{m}_i}{4\pi^2 U} e^{\left(\frac{\phi_i^2}{U} + i\phi_i n_i + \frac{\mathbf{m}_i^2}{U} - 2\mathbf{m}_i\cdot\vec{s}_i\right)}.$$

The partition function now becomes

$$Z = \int \prod_i \frac{\mathrm{d}\bar{c}_i \mathrm{d}c_i \mathrm{d}\phi_i \mathrm{d}\mathbf{m}_i}{4\pi^2 U} e^{\left(-\int_0^\beta \mathcal{L}(\tau)\right)},$$

$$\mathcal{L}(\tau) = \sum_{i\sigma} \bar{c}_{i\sigma}(\tau)\partial_\tau c_{i\sigma}(\tau) + H_0(\tau) + \mathcal{L}_{int},$$

$$\mathcal{L}_{int} = \sum_i \left[\frac{\phi_i^2}{U} + i\phi_i n_i + \frac{\mathbf{m}_i^2}{U} - 2\mathbf{m}_i\cdot\vec{s}_i\right].$$

To make progress we need two approximations: i) neglect the time (τ) dependence of the HS fields treating them as classical, and ii) fully retain the thermal fluctuations in $\mathbf{m}_i$, but treat ϕ_i at the saddle point level, *i.e.*, $\phi_i \to \langle\phi_i\rangle = (U/2)\langle\langle n_i\rangle\rangle = U/2$ at half-filling. With this approximation the half-filled problem is mapped on to non-interacting electrons coupled to the field $\mathbf{m}_i$. Substituting these, and simplifying the action, one gets the effective Hamiltonian

$$H_{eff} = \sum_{ij,\sigma} t_{ij} c^\dagger_{i\sigma} c_{j\sigma} - \tilde{\mu}N - \frac{U}{2}\sum_i \mathbf{m}_i\cdot\vec{\sigma}_i + \frac{U}{4}\sum_i \mathbf{m}_i^2, \quad (2)$$

where $\tilde{\mu} = \mu - U/2$. We have redefined $\mathbf{m}_i \to \frac{U}{2}\mathbf{m}_i$, so that the $\mathbf{m}_i$ is dimensionless.

We can write $H_{eff} = H_{el}\{\mathbf{m}_i\} + H_{cl}$, where $H_{cl} = (U/4)\sum_i \mathbf{m}_i^2$. For a *given* configuration $\{\mathbf{m}_i\}$ one just needs to diagonalize H_{el}, but the $\{\mathbf{m}_i\}$ themselves have to be determined from the distribution

$$P\{\mathbf{m}_i\} \propto \mathrm{Tr}_{c,c^\dagger} e^{-\beta H_{el}} e^{-\beta H_{cl}}. \qquad (3)$$

Equation (2) describes electron propagation in the $\mathbf{m}_i$ background, while eq. (3) describes how the $\mathbf{m}_i$ emerge and are spatially correlated due to electron motion. The neglect of dynamics in the $\mathbf{m}_i$ reduces the method to unrestricted Hartee-Fock (UHF) mean-field theory at $T = 0$. However, the exact inclusion of classical thermal fluctuations quickly improves the accuracy of the method with

increasing temperature. We will discuss the limitations of the method further on.

Due to the fermion trace, $P\{\mathbf{m}_i\}$ is not exactly calculable. To generate the equilibrium $\{\mathbf{m}_i\}$ configurations we use Monte Carlo (MC) sampling [37–39]. Computing the energy cost of an attempted update requires diagonalizing H_{el}. To access large sizes within limited time, we use a cluster algorithm [40] for estimating the update cost. Rather than diagonalize the full H_{eff} for every attempted update, we calculate the energy cost of an update by diagonalizing a cluster of size N_c around the reference site. We have extensively benchmarked this cluster based MC method [40]. Most of our results are based on MC on $N = 24 \times 24$ lattices, with clusters of size $N_c = 8 \times 8$. We will comment on our size dependence checks at the end of the paper. We calculate the thermally averaged structure factor $S(\mathbf{q}) = \frac{1}{N^2}\sum_{ij}\langle \mathbf{m}_i \cdot \mathbf{m}_j\rangle e^{i\mathbf{q}\cdot(\mathbf{R}_i-\mathbf{R}_j)}$ at each temperature. The onset of rapid growth in $S(\mathbf{q})$ at some $\mathbf{q} = \mathbf{Q}$, say, indicates a magnetic transition. The electronic properties are calculated by diagonalizing H_{el} on the full lattice for equilibrium $\{\mathbf{m}_i\}$ configurations.

We present our results in the following sequence. We start with the phase diagram, summarising the magnetic, transport and spectral character that emerges from the detailed calculation. Following this we discuss the temperature dependence of the d.c. resistivity, since it defines our transport classification. We then look at the optical conductivity and correlate its features with the single-particle density of states (DOS) as the system is driven across the Mott transition. While the transport and DOS are insensitive to the detailed nature of magnetic fluctuations, the *angle-resolved photoemission spectrum* (ARPES) depends crucially on the non-local magnetic correlations. The last and central part of our presentation deals with the angular dependence in the ARPES and its relation to magnetic correlations on the frustrated structure.

Results. – Figure 1 shows the U-T phase diagram at $t'/t = 0.8$. Let us first discuss the ground state. Our $T = 0$ result is equivalent to UHF and leads to a transition from an uncorrelated paramagnetic metal to an AF metal with wave vector $\mathbf{Q} = \mathbf{Q}_1 \sim \{0.85\pi, 0.85\pi\}$ at $U_{c1} \sim 4.0t$. At $U_{c2} \sim 4.4t$ there is a transition to an AF insulator with $\mathbf{Q}_2 \sim \{0.83\pi, 0.83\pi\}$. At large U/t, this evolves into slightly away from Néel state with $\mathbf{Q}_2 \sim \{0.8\pi, 0.8\pi\}$.

The magnitude $m_i = |\mathbf{m}_i|$ is small in the AFM and grows as U/t increases in the Mott phase. The existence of the AF metal, and the nature of order in the intermediate U/t Mott phase, could be affected by the neglected quantum fluctuations of the $\mathbf{m}_i$ [41].

Finite temperature brings into play the low-energy fluctuations of the $\mathbf{m}_i$. The effective model has the $O(3)$ symmetry of the parent Hubbard model so it cannot sustain true long-range order at finite T. However, our annealing results suggest that magnetic correlations grow rapidly below a temperature T_{corr}, and weak inter-planar coupling would stabilize in plane order below T_{corr} (equivalent

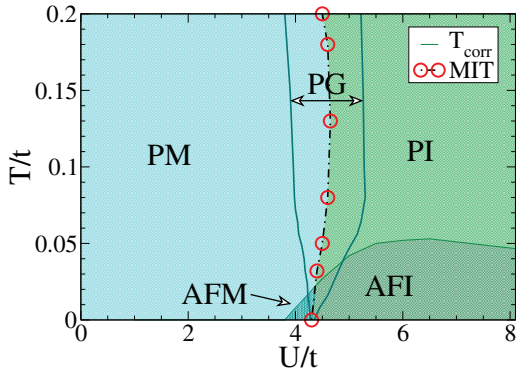

Fig. 1: (Colour on-line) U-T phase diagram of the Hubbard model at $t'/t = 0.8$. The phases are paramagnetic metal (PM), paramagnetic insulator (PI), antiferromagnetic metal (AFM) and antiferromagnetic insulator (AFI). The AFM and AFI are not simple Néel ordered (see text). PG indicates a pseudogap phase, metallic or insulating. There is no genuine magnetic transition in two dimensions so our T_{corr} indicates the temperature across which the magnetic correlation length grows rapidly (see text). The MIT line is determined from change in sign of the temperature derivative of resistivity, *i.e.*, $\mathrm{d}\rho/\mathrm{d}T = 0$.

results for the classical Heisenberg model are discussed in Takahashi [42]). This T_{corr} increases from zero at $U = U_{c1}$, reaches a peak at $U/t \sim 6.5$, and falls beyond as the kinetic energy gain from virtual hops decreases. Note that unlike mean-field theory we can describe a magnetically disordered (Mott) insulating phase since the auxiliary fields $\mathbf{m}_i$ survive even after spatial order is lost.

We classify the finite T phases as metal when $\mathrm{d}\rho/\mathrm{d}T > 0$ and insulator when $\mathrm{d}\rho/\mathrm{d}T < 0$. The dotted line indicating the MIT corresponds to the locus $\mathrm{d}\rho(T,U)/\mathrm{d}T = 0$. In addition to the magnetic and transport classification we also show a window around the MIT line where the electronic density of states (DOS) has a pseudogap. To the right of this region the DOS has a "hard gap" while to the left the DOS is featureless. The MIT line shows reentrant insulator-metal-insulator behavior with increasing T near $U \sim U_{c2}$. On the overall scale of fig. 1 only a mild concavity is visible in the metal-insulator phase boundary. We will discuss this feature in detail elsewhere [43] and compare to the organic experiments.

Figure 2 shows the resistivity $\rho(T)$ computed via the Kubo formula for varying U/t. The optical conductivity $\sigma(\omega)$ of the two-dimensional system is given by [44]

$$\sigma^{xx}_{2D}(\omega) = \frac{\sigma_0}{N}\sum_{\alpha,\beta}\frac{n_\alpha - n_\beta}{\epsilon_\beta - \epsilon_\alpha}|\langle\alpha|J_x|\beta\rangle|^2\delta(\omega - (\epsilon_\beta - \epsilon_\alpha)),$$

where the current operator J_x is

$$J_x = -i\sum_{i,\sigma}\Big[t(c^\dagger_{i,\sigma}c_{i+\hat{x},\sigma} - \text{h.c.}) + t'(c^\dagger_{i,\sigma}c_{i+\hat{x}+\hat{y},\sigma} - \text{h.c.})\Big],$$

$n_\alpha = f(\epsilon_\alpha)$ is the Fermi function, and ϵ_α and $|\alpha\rangle$ are, respectively, the single-particle eigenvalues and eigenstates

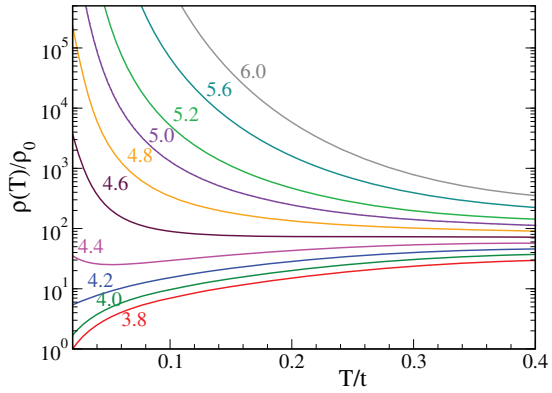

Fig. 2: (Colour on-line) Temperature dependence of the resistivity for different U near the M-I transition. The normalizing scale is $\rho_0 = \hbar/\pi e^2$ (see text). The U/t values are indicated on the curves.

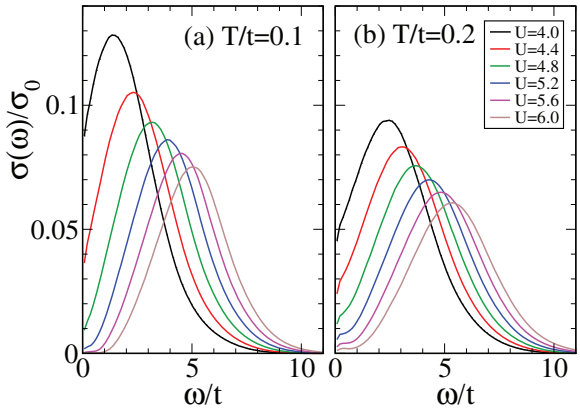

Fig. 3: (Colour on-line) Optical conductivity at $T/t = 0.1$ and 0.2 for U varying across U_c. At these temperatures the $\sigma(\omega)$ is non-Drude even in the "weakly correlated" case $U/t \sim 4.0$. The finite frequency peak evolves into the Hubbard transition at large U/t.

of H_{eff} in a given background $\{\mathbf{m}_i\}$. The d.c. conductivity is the $\omega \to 0$ limit of $\sigma^{xx}_{2D}(\omega)$. $\sigma_0 = \frac{\pi e^2}{\hbar}$, the scale for two-dimensional conductivity, has the dimension of *conductance*. Our results are averaged over ~ 20 equilibrium MC configurations. We have verified the f-sum rule numerically for the optical conductivity.

As $T \to 0$ the resistivity $\rho(T)$ goes either to zero (for $U < U_{c2} \sim 4.4t$) or diverges (for $U > U_{c2}$). The $T \to 0$ behaviour for U very close to U_{c2} is, however, difficult to settle numerically with finite annealing time. The seemingly finite $\rho(0)$ in the metal arises from the survival of a few finite m_i which should all ideally vanish as $T \to 0$.

We make the following observations about the finite T resistivity: i) For $U \gg U_{c2}$ the prominent Mott gap leads to $\mathrm{d}\rho/\mathrm{d}T < 0$ over the entire temperature window. However, just beyond U_{c2}, for $(U_{c2} - U) \ll U_{c2}$, we observe non-monotonic $\rho(T)$: at the lowest temperature we have $\mathrm{d}\rho/\mathrm{d}T < 0$, which then crosses over to $\mathrm{d}\rho/\mathrm{d}T > 0$ and at even higher T to another weakly $\mathrm{d}\rho/\mathrm{d}T < 0$ regime! This re-entrant behaviour is hard to make out on the log scale in fig. 2 and we will discuss it elsewhere [43]. ii) In the metallic phase, $U < U_{c2}$, the resistivity arises from thermally generated magnetic fluctuations. Within a perturbative scheme the scattering rate is $\propto \langle m_i^2 \rangle \sim T$. A full treatment including the quantum effects in $\mathbf{m}_i$ may lead to a Fermi liquid T^2 behaviour. However, at higher T the classical thermal fluctuations should provide an adequate description of the transport.

Figure 3 shows the optical conductivity $\sigma(\omega)$ at $T = 0.1t$ and $T = 0.2t$ as U/t is varied across the Mott crossover. The following are our main observations. i) There is a distinctly non-Drude character to $\sigma(\omega)$ in the metal, $U/t \lesssim 4.4$, with $\mathrm{d}\sigma(\omega)/\mathrm{d}\omega|_{\omega\to 0} > 0$. ii) The low frequency hump in this "bad metal" evolves into the interband Hubbard peak, at a frequency $\omega \sim U\bar{m}$ in the Mott phase, as increasing U in panels (a), (b) reveal. iii) The change in the lineshape with increasing T is more prominent in the metal, with the peak location moving outward,

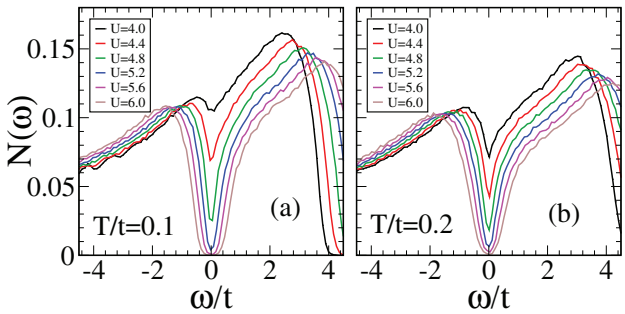

Fig. 4: (Colour on-line) Density of states at $T/t = 0.1$, 0.2 for U varying across U_c. The dip in the DOS deepens with increasing T for $U/t \lesssim 4.6$. For larger U/t the system slowly gains spectral weight with increasing T.

and is more modest deep in the insulator. iv) The temperature dependence of the low-frequency optical weight, at $\omega \lesssim 0.2t$, is different on the two sides of the Mott crossover. In the lower U/t "metal" the large Drude weight at low T decreases quickly with increasing T while at larger U/t, in the insulator, the low frequency weight increases somewhat with increasing T.

The crossover from the "bad metal" to the insulator involves a wide window with a pseudogap in the electronic DOS, $N(\omega)$. One may have guessed this from the depleting low frequency weight in $\sigma(\omega)$, fig. 4 makes this feature explicit. Our results indicate a wide interaction window, $U/t \sim 4$–5.3, where there is a distinct pseudogap in the global DOS for $T \gtrsim 0.05t$. For $U/t \lesssim 4.6$ the dip feature deepens with increasing T, we have $\mathrm{d}N(0)/\mathrm{d}T < 0$ (compare panels (a) and (b), fig. 4), while for $U/t \gtrsim 4.6$ we have a weak $\mathrm{d}N(0)/\mathrm{d}T > 0$. The PG arises from the coupling of electrons to the fluctuating $\mathbf{m}_i$. A large m_i at all sites would open a Mott gap, independent of any order among the moments. Weaker m_i, thermally generated in the metal near U_{c1} and with only short-range correlations,

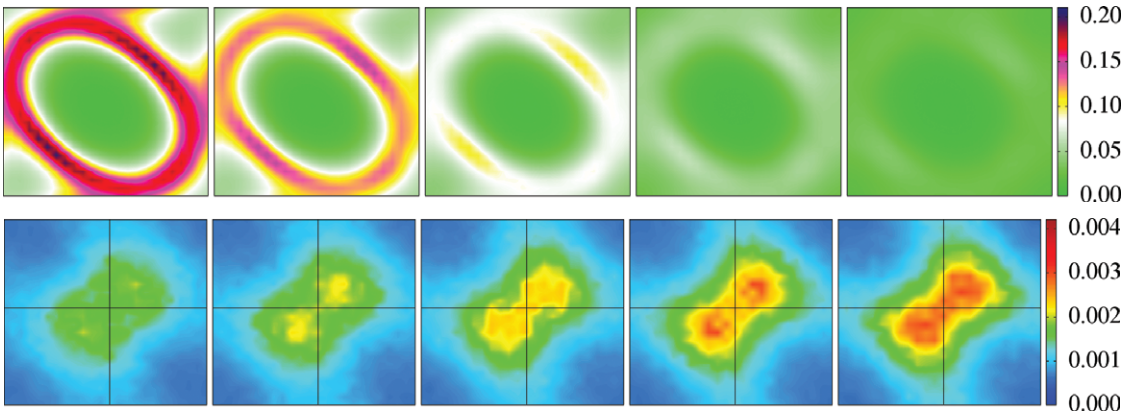

Fig. 5: (Colour on-line) Top: momentum dependence of the low-frequency spectral weight in the electronic spectral function $A(\mathbf{k},\omega=0)$ showing its anisotropy, at $T/t=0.1$, and $U/t=4.2,4.4,4.6,4.8,5.0$, left to right. k_x,k_y range from $[-\pi,\pi]$ in the panels. Note the systematically larger weight near $\mathbf{k}=[\frac{\pi}{2},\frac{\pi}{2}]$ and $[\frac{-\pi}{2},\frac{-\pi}{2}]$ and smaller weight in the segments near $[\pi,0]$ and $[0,\pi]$. Bottom: magnetic structure factor $S(\mathbf{q})$ for the auxiliary fields $\mathbf{m}_i$ for the same set of U/t. The q_x,q_y range from $[0,2\pi]$. Note the very weak and diffuse structure at $U/t=4.2$ and the much larger and differentiated structure at $U/t=5.0$.

manages to deplete low frequency weight without opening a gap. Since the typical size $\langle m_i\rangle$ increases with T in the metal, we see the dip deepening at $U<U_c$.

We extract the thermal and spin averaged spectral function $A(\mathbf{k},\omega)$ as follows. The retarded Green's function $G_\sigma(\mathbf{k},t)=-i\theta(t)\langle\{c_{\mathbf{k}\sigma}(t),c^\dagger_{\mathbf{k}\sigma}(0)\}\rangle$ can be simplified to $G_\sigma(\mathbf{k},t)=-i\theta(t)\sum_\alpha|\langle\mathbf{k}\sigma|\alpha\rangle|^2e^{-i\epsilon_\alpha t}$ where $\{|\alpha\rangle\}$ are the single-particle eigenstates and ϵ_α are eigenvalues in a given $\{\mathbf{m}_i\}$ background. In the frequency domain, this becomes

$$G_\sigma(\mathbf{k},\omega)=\sum_\alpha\frac{|\langle\mathbf{k}\sigma|\alpha\rangle|^2}{\omega-\epsilon_\alpha+i0^+}.$$

The spectral function is $A_\sigma(\mathbf{k},\omega)=-\frac{1}{\pi}\mathrm{Im}G_\sigma(\mathbf{k},\omega)=\sum_\alpha|\langle\mathbf{k}\sigma|\alpha\rangle|^2\delta(\omega-\epsilon_\alpha)$. We average this over the thermal $\{\mathbf{m}_i\}$ configurations and electron spin σ.

Figure 5, top row, shows maps of $A(\mathbf{k},0)$ in k_x,k_y plane at $T/t=0.1$, as increasing U/t transforms the bad metal to a Mott insulator. The first panel at $U/t=4.2$ shows weak anisotropy on the nominal FS while fig. 4(a) suggests that a weak PG has already formed. At $U/t=4.4$, next panel, the weak anisotropy is much amplified and the weight in the $[0,0]\to[\pi,\pi]$ direction is distinctly larger.

The next three panels basically show insulating states but without a hard Mott gap. Overall, the "destruction" of the FS seems to start near $[\pm\pi,0]$ and $[0,\pm\pi]$, the "hot" regions, and ends with the region near $[\pi/2,\pi/2]$, etc., the "cold spots".

Second row in fig. 5 shows the $S(\mathbf{q})$ of the auxiliary fields at $T/t=0.1$ for the same U/t as in the upper row. While there is no magnetic order we can see the growth of correlations centered around $\mathbf{Q}\approx[0.85\pi,0.85\pi]$ as U/t increases. The dominant electron scattering would be from $\mathbf{k}$ to $\mathbf{k}+\mathbf{Q}$, and the impact would be greatest in regions of the FS in the proximity of minima in $|\nabla\epsilon_\mathbf{k}|$ (which correspond to large DOS). The location of the hot spots on the FS, and the momentum connecting them, indeed correspond to this scenario.

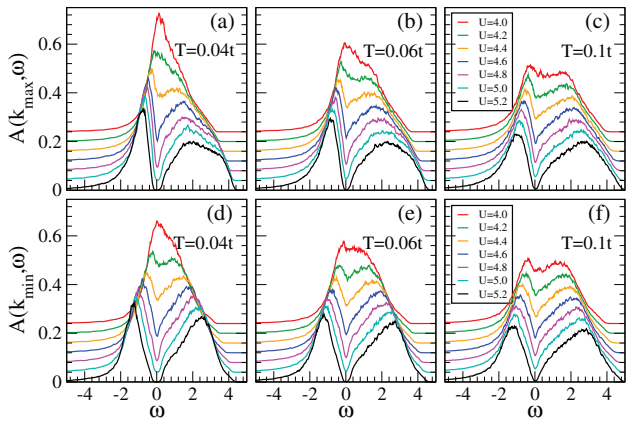

Fig. 6: (Colour on-line) The spectral function $A(\mathbf{k},\omega)$ at two $\mathbf{k}$ points on the FS that correspond to the highest and lowest value of $A(\mathbf{k},0)$. We highlight the anisotropy over a range of U/t values, as the system evolves from a moderately damped metal to a pseudogap phase, and three temperatures.

The full spectral function at the "cold spot" and "hot spot", where $A(\mathbf{k},0)$ is maximum and minimum, are shown, respectively, in the top and bottom panels in the fig. 6. At $T=0.1t$, panels (c) and (f), for which $A(\mathbf{k},0)$ is shown in fig. 5, there is no quasiparticle (QP) peak in $A(\mathbf{k},\omega)$ at either the cold or hot spot for the U range shown. The k_{max} and k_{min} data differ only quantitatively. At lower T and weaker U, however, the cold spot shows a QP peak while a pseudogap feature is already visible at the hot spot. However, as we will see next, the lower T result may be less reliable, due to missing dynamics of $\mathbf{m}_i$.

Discussion. – We wish to quickly touch upon four issues.

i) *The limitations of our method*: While we capture nontrivial spatial correlations and its impact on electronic properties, caution is in order about the following: a) Neglecting the dynamics of the $\mathbf{m}_i$ misses correlation

effects, beyond UHF, in the ground state of the metal and underestimates U_c/t. b) It misses possible "Fermi liquid" physics in the low T metal. Near the MIT it is useful to think of the metal, crudely, in terms of a self generated Kondo scale T_K^*, so that for $T > T_K^*$ the dynamics of $\mathbf{m}_i$ is not crucial [45]. As a rough measure we would suggest that our frequency dependent results would be valid for $|\omega| > T_K^*$ when $T < T_K^*$, and all the way down to $\omega = 0$ when $T > T_K^*$. $T_K^* \sim 0.1t$ can be considered as an upper limit for the U/t window we have focused on. c) There could be a "spin liquid" insulator at intermediate U/t as suggested [27,28] $t'/t = 1$. We would prefer to emphasize our finite T results rather than the detailed nature of the ground state.

ii) *Checks on size dependence*: While thermodynamic features and the overall DOS can be reasonably accessed even on small system size, the ARPES can be significantly size dependent. We have checked the MC results for sizes $L \times L$, with $L = 8, 12, 16, 20, 24, 30$ to establish that our results represent the $L \to \infty$ limit.

iii) *Connection to experiments*: This paper has deliberately focused on results arising from the model without attempting a comparison with data on the organics. Our preprint [46] provided a detailed comparison on the resistivity and optical conductivity. We will discuss these transport features, as well as the re-entrance aspect in the M-I phase diagram, in a separate paper [43].

iv) *Effect of varying t'/t*: While U_c depends strongly on t'/t, varying from $U_c/t \to 0$ as $t' \to 0$, to $U_c/t \sim 5$ as $t' \sim t$, the PG width doesn't vary significantly. The magnetic character of the insulating phase changes from Néel to spiral around $t'/t \sim 0.7$.

Conclusion. – We introduced and explored in detail a method which retains the spatial correlations that are crucial near the Mott transition on a frustrated lattice. For the anisotropic-triangular-lattice Hubbard model at half-filling we find that increasing interaction strength leads to a wide pseudogap window and non-Drude response in the optical conductivity near the Mott transition. The angle-resolved spectral function reveals that the coupling of electrons to the non-local magnetic fluctuations leads to a strong and distinctive momentum dependence of quasiparticle damping and pseudogap formation as the Mott transition is approached.

* * *

We acknowledge use of the HPC clusters at HRI. PM acknowledges support from the DST India (Athena), a DAE-SRC Outstanding Research Investigator grant, and a discussion with T. V. Ramakrishnan.

REFERENCES

[1] Mott N. F., *Metal-Insulator Transitions* (Taylor and Francis) 1990.
[2] Georges A. *et al.*, *Rev. Mod. Phys.*, **68** (1996) 13.
[3] Imada M. *et al.*, *Rev. Mod. Phys.*, **70** (1998) 1039.
[4] Dagotto E., *Rev. Mod. Phys.*, **66** (1994) 763.
[5] Ong N. P. and Cava R. J., *Science*, **305** (2005) 52.
[6] Balents L., *Nature*, **464** (2010) 199.
[7] Kanoda K. and Kato R., *Annu. Rev. Condens. Matter Phys.*, **2** (2011) 167; Powell B. J. and McKenzie R. H., *Rep. Prog. Phys.*, **74** (2011) 056501.
[8] Kandpal H. C. *et al.*, *Phys. Rev. Lett.*, **103** (2009) 067004; Shimizu Y. *et al.*, *J. Phys. Soc. Jpn.*, **80** (2011) 074702.
[9] Lefebvre S. *et al.*, *Phys. Rev. Lett.*, **85** (2000) 5420; Kagawa F. *et al.*, *Phys. Rev. B*, **69** (2004) 064511.
[10] Yasin S. *et al.*, *Eur. Phys. J. B*, **79** (2011) 383.
[11] Merino J. *et al.*, *Phys. Rev. Lett.*, **100** (2008) 086404.
[12] Dumm M. *et al.*, *Phys. Rev. B*, **79** (2009) 195106.
[13] Powell B. J. *et al.*, *Phys. Rev. B*, **80** (2009) 054505.
[14] Kawamoto A. *et al.*, *Phys. Rev. B*, **52** (1995) 15522.
[15] Tocchio L. F. *et al.*, *Phys. Rev. B*, **87** (2013) 035143.
[16] Morita H. *et al.*, *J. Phys. Soc. Jpn.*, **71** (2002) 2109.
[17] Watanabe T. *et al.*, *Phys. Rev. B*, **77** (2008) 214505.
[18] Inaba K. *et al.*, *J. Phys.: Conf. Ser.*, **150** (2009) 042066.
[19] Tocchio L. F. *et al.*, *Phys. Rev. B*, **80** (2009) 064419.
[20] Limelette P. *et al.*, *Phys. Rev. Lett.*, **91** (2003) 016401.
[21] Aryanpour K. *et al.*, *Phys. Rev. B*, **74** (2006) 085117.
[22] Galanakis D. *et al.*, *Phys. Rev. B*, **79** (2009) 115116.
[23] Parcollet O. *et al.*, *Phys. Rev. Lett.*, **92** (2004) 226402.
[24] Ohashi T. *et al.*, *Phys. Rev. Lett.*, **100** (2008) 076402.
[25] Liebsch A. *et al.*, *Phys. Rev. B*, **79** (2009) 195108.
[26] Sato T., Hattori K. and Tsunetsugu H., *J. Phys. Soc. Jpn.*, **81** (2012) 083703; *Phys. Rev. B*, **86** (2012) 235137.
[27] Sahebsara P. and Senechal D., *Phys. Rev. Lett.*, **100** (2008) 136402.
[28] Yang H. Y. *et al.*, *Phys. Rev. Lett.*, **105** (2010) 267204.
[29] Clay R. T. *et al.*, *Phys. Rev. Lett.*, **101** (2008) 166403.
[30] Watanabe T. *et al.*, *J. Phys. Soc. Jpn.*, **75** (2006) 074707.
[31] Kyung B. and Tremblay A.-M. S., *Phys. Rev. Lett.*, **97** (2006) 046402.
[32] Liu J. *et al.*, *Phys. Rev. Lett.*, **94** (2005) 127003.
[33] Hubbard J., *Phys. Rev. Lett.*, **3** (1959) 77.
[34] Schulz H. J., *Phys. Rev. Lett.*, **65** (1990) 2462.
[35] Weng Z. Y. *et al.*, *Phys. Rev. B*, **43** (1991) 3790.
[36] Borejsza K. and Dupuis N., *Europhys. Lett.*, **63** (2003) 722.
[37] Mayr M. *et al.*, *Phys. Rev. B*, **73** (2006) 014509.
[38] Dagotto E. *et al.*, *Phys. Rep.*, **344** (2001) 1.
[39] Dubi Y., Meir Y. and Avishai Y., *Nature*, **449** (2007) 876.
[40] Kumar S. and Majumdar P., *Eur. Phys. J. B*, **50** (2006) 571.
[41] Yang H. Y. *et al.*, *Phys. Rev. Lett.*, **105** (2010) 267204.
[42] Takahashi M., *Phys. Rev. B*, **36** (1987) 3791.
[43] Tiwari R. and Majumdar P., in preparation.
[44] Allen P. B., in *Conceptual Foundation of Materials*, edited by Louie S. G. and Cohen M. L., Vol. **2** (Elsevier) 2006.
[45] Bulla R., *Phys. Rev. Lett.*, **83** (1999) 136.
[46] Tiwari R. and Majumdar P., arXiv:1301.5026.